

OPTICAL FIBRES AND WAVEGUIDES

PACS numbers: 42.81.Cn; 33.50.Dq
DOI: 10.1070/QE2010v040n02ABEH014198

Luminescent properties of bismuth centres in aluminosilicate optical fibres

L.I. Bulatov, V.M. Mashinsky, V.V. Dvoyrin, E.F. Kustov, E.M. Dianov

***Abstract*. The shape and spectral position of the luminescence bands of bismuth-doped aluminosilicate glass fibres are shown to depend on excitation power and wavelength. This indicates that the red and IR luminescence bands are composed of several components. The absorption and radiative transitions involved are identified, and a diagram of energy levels and transitions is obtained for four modifications of a bismuth centre in different environments in the aluminosilicate glass network. The effect of local environment on the optical properties of the bismuth centres is examined.**

Keywords: *bismuth centres, active optical fibres, luminescence.*

1. Introduction

Broadband IR luminescence in various glasses and optical fibres lightly doped with bismuth is due to active bismuth centres (ABCs) and opens up new possibilities of mastering the second and third transmission windows of optical fibre communication systems. Very recently, bismuth-doped aluminosilicate and phosphogermanosilicate fibre lasers have been demonstrated to operate in the range 1150 – 1550 nm [1 – 3]. The slope efficiency of the bismuth-doped fibre lasers is however rather low (within 30 % at room temperature) compared to rare-earth-doped fibre lasers [2 – 4].

Despite the intense recent research, no model of bismuth centres that would adequately describe the spectroscopic properties of bismuth-doped glasses has been constructed to date. The proposed sources of the IR luminescence (bands in the range 1150 – 1430 nm) and red luminescence (band at 740 nm) include Bi^+ [5], Bi^{2+} [6] and Bi^{5+} [7] ions; neutral and negatively charged dimers, such as Bi_2, Bi_2^- and Bi_2^{2-} [8, 9]; the BiO molecule [10, 11]; and $\{[AlO_{4/2}]^-, Bi^+\}$ [12] and BiO_4 [13] complexes. The red luminescence may originate from Bi^{2+} [14, 15] and Bi^{5+} [16]. Note that the IR and red luminescences may be due to both the same ionic bismuth species [13, 16] and different ions [14, 15]. A number of reports examined the possibility that the glass contained several ionic bismuth species [14] or several configurations of an ion in different environments [5].

This paper presents a continuation of our studies of ABCs in aluminosilicate glass fibres [17]. Here we examine the effect of excitation power and wavelength on the luminescent properties of ABCs and demonstrate that there are four modifications of an ABC which have the same structure of absorption and luminescence bands.

2. Samples and measurement procedure

Given that several aluminosilicate glass fibres differing in the composition of their bismuth-doped core (sample 25: molar ratio $SiO_2 : Al_2O_3 = 95.8 : 4.2$; sample 35: $SiO_2 : Al_2O_3 : GeO_2 : P_2O_5 = 93.2 : 4.25 : 1.5 : 1.05$; sample 50: $SiO_2 : Al_2O_3 : GeO_2 = 95.4 : 3.6 : 1.0$ [17]) were shown to have essentially identical luminescence spectra at a given excitation wavelength, we report here further characterisation of one of them (sample 50). The fibre was fabricated by the modified chemical vapour deposition (MCVD) process. The bismuth content of its core was within 0.02 at %. The outer diameter of the fibre was 125 μm, and the core diameter was 8 μm. To examine the effect of the drawing process, we also studied a fibre preform with a core diameter of 1 mm.

The excitation beam was launched into one of the ends of the fibre and preform. The luminescence spectrum of the fibre was measured using the output beam. To reduce the reabsorption-induced distortion of the spectrum, the fibre length was 1 to 10 cm (depending on the spectral region). The fibre absorbed ~ 10 % of the excitation beam power. The luminescence spectrum of the preform was taken in a 90° geometry. When the luminescence spectra were measured at different excitation wavelengths, the input beam power was maintained constant.

The excitation sources used were $Kr^+ – Ar^+$ (454 – 676.4 nm), Ti^{3+} : sapphire (730 – 855 nm) and Nd^{3+} : YAG (1064 nm) lasers, laser diodes (900 and 970 nm) and a Raman fibre laser (1350 nm). The luminescence spectra were measured in the range 600 – 1700 nm at room temperature using an Ando Model 6317 spectrophotometer. The absorption spectrum of the fibre is presented in Fig. 1 (the arrows mark the excitation wavelengths).

L.I. Bulatov Department of Physics, M.V. Lomonosov Moscow State University, Vorob'evy gory, 119992 Moscow, Russia; e-mail: lenar@fo.gpi.ru;
V.M. Mashinsky, V.V. Dvoyrin, E.M. Dianov Fiber Optics Research Center, Russian Academy of Sciences, ul. Vavilova 38, 119333 Moscow, Russia; e-mail: vmm@fo.gpi.ru;
E.F. Kustov Moscow Power Engineering Institute, Krasnokazarmennaya ul. 14, 111250 Moscow, Russia

Received 28 July 2009
Kvantovaya Elektronika **40** (2) 153 – 159 (2010)
Translated by O.M. Tsarev

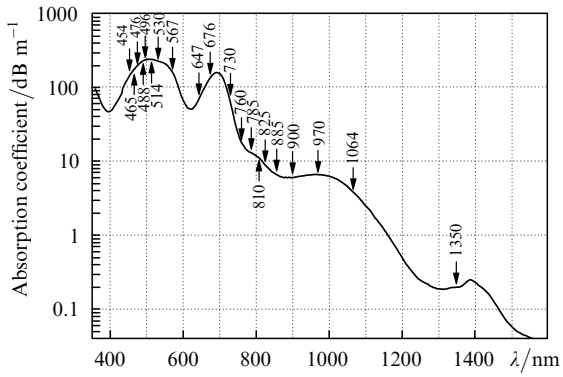

Figure 1. Optical loss spectrum of the fibre. The arrows mark the excitation wavelengths used in luminescence measurements.

3. Results and discussion

Luminescence intensity saturation was explored at two excitation wavelengths, 514 and 647 nm. At low excitation powers, the intensity of the red luminescence is lower than that of the IR luminescence, but with increasing excitation power the former rises more rapidly and the red luminescence becomes predominant (Fig. 2). Similar behaviour of the Bi luminescence was reported by Qiu and Shen [15].

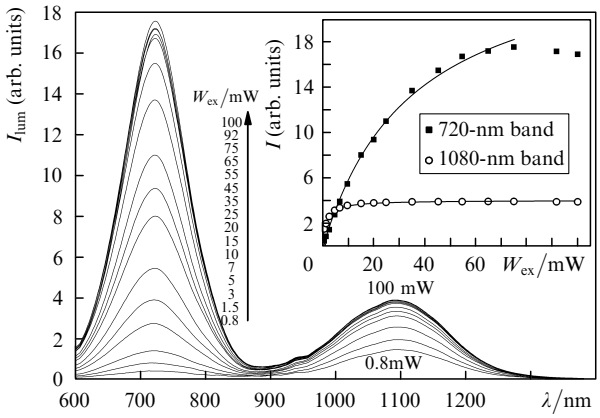

Figure 2. Effect of 514-nm excitation power, W_{ex}, on the luminescence spectrum of the fibre. Inset: red and IR peak luminescence intensities as functions of excitation power.

The saturation intensities I_s obtained by fitting the peak luminescence intensity L as a function of excitation intensity I to an equation of the form $L \sim I/(1 + I/I_s)$ are 70 ± 5.7 and 3 ± 0.12 kW cm^{-2} for the red and IR luminescence bands, respectively, under excitation at 514 nm and 65.6 ± 5.6 and 8.7 ± 1.4 kW cm^{-2} under 647-nm excitation.

In addition, the excitation power influences the spectral shape of the bands (Fig. 3). With increasing excitation power, the width of the red luminescence band decreases by 30 %, with no changes in its peak position. The reduction in bandwidth and the constant peak position under saturation conditions suggest that the band comprises at least three components. With increasing input beam power at 514 and 647 nm, the relative intensity of the central component (742 nm) increases with respect to the other two components (685 and 810 nm) [17]. In contrast to that of the red luminescence, the maximum of the IR luminescence band shifts by 40 nm with increasing excitation power. This is due to the intensity redistribution between the components at 1078 and 1148 nm: excitation at 647 nm increases the relative intensity of the longer wavelength component (Fig. 3), whereas excitation at 514 nm increases that of the shorter wavelength component.

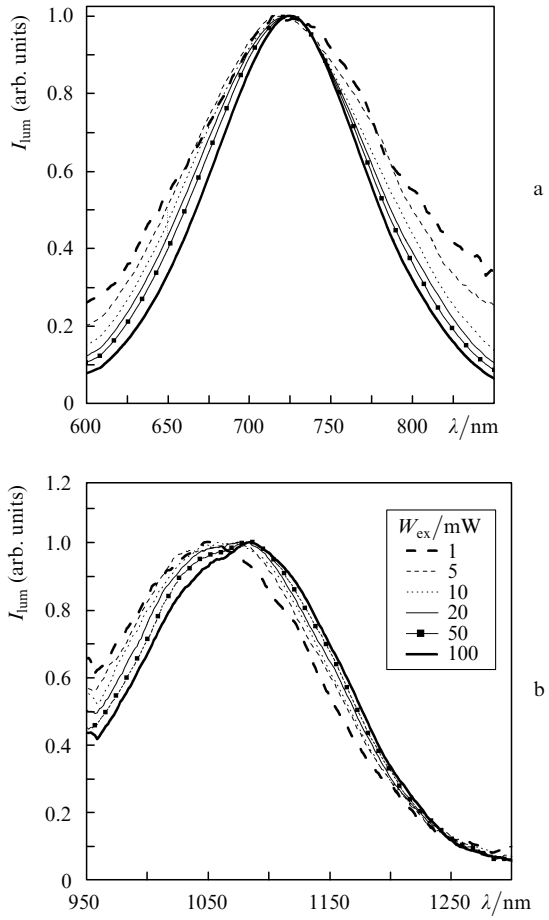

Figure 3. Effect of excitation power on the shape of the luminescence bands of the fibre: $\lambda_{ex} = 514$ (a) and 647 nm (b).

Thus, the observed effect of excitation power on the luminescence spectrum of the fibre indicates that the red and IR luminescence bands have a complex structure, as supported by earlier fitting results for the luminescence spectra [17].

Figure 4 illustrates the effect of excitation wavelength on the luminescence spectra of the fibre and preform at a fixed excitation power. The spectra are seen to differ from one another (especially at excitation wavelengths in the range 730–810 nm). Some of the luminescence spectra of the preform show a feature at 900 nm, in contrast to the spectra of the fibre, and the bands centred at 1070, 1160 and ~ 1350 nm are markedly stronger in the spectra of the preform. Of special note is the strong luminescence band centred at 810 nm, which is present in the spectra of both the fibre and preform at excitation wavelengths from 760 to 810 nm.

Significant distinctions between the luminescence spectra of fibres and preforms were observed earlier by Razdobreev et al. [18] and Truong et al. [19], and were attributed to the

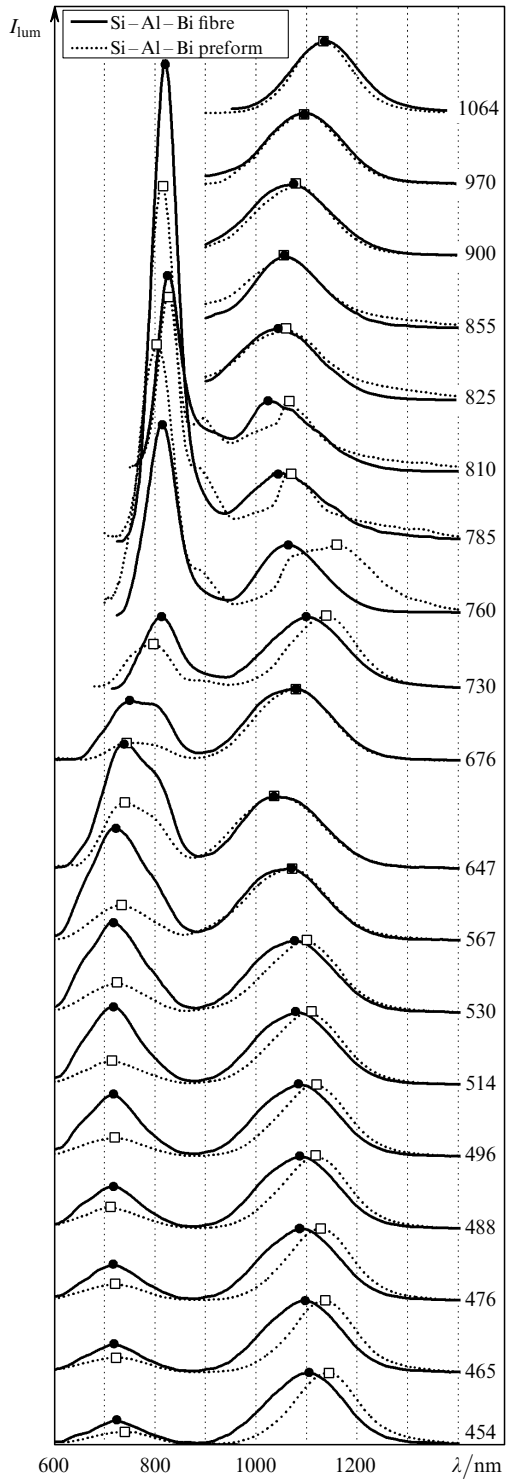

Figure 4. IR-band-normalised luminescence spectra of the fibre and preform. The numbers at the spectra specify the excitation wavelength in nanometres. The points mark the maxima of the luminescence bands of the fibre (●) and preform (□).

effect of the high-temperature processing of the preforms in an oxygen-free environment in the course of fibre drawing. However, given that the substrate tube collapse and fibre drawing processes are similar in thermal conditions, it seems likely that a more important cause of the observed distinctions between the spectra is the cooling rate during fibre drawing, which is several orders of magnitude higher than that of the preform glass (because of the much smaller diameter of the fibre, 0.125 against $\sim$ 15 mm, and its larger surface area). This leads to an increase in the fictive temperature of the glass by 300 – 400 K, i.e., to the 'freezing' of the fibre glass structure, which is much more disordered compared to the preform.

The excitation wavelength also influences the luminescence band position. In particular, the red luminescence band may shift from 715 to 825 nm, and the IR band, from 1087 to 1137 nm (Fig. 4). In addition to changes in band shape and position, the excitation wavelength influences the intensity of the red luminescence components relative to the IR luminescence intensity (Fig. 5). The widths of the 740- and 810-nm bands grow as the excitation wavelength increases from 454 to 647 and from 676 to 785 nm, respectively. The monotonic increase in red luminescence intensity with excitation wavelength in the range $\sim 450 - 650$ nm is inconsistent with the hypothesis that the red luminescence is due to Bi^{2+} [14, 15] because the Bi^{2+} luminescence excitation spectrum is composed of two, well-resolved bands at 470 and 590 nm [20].

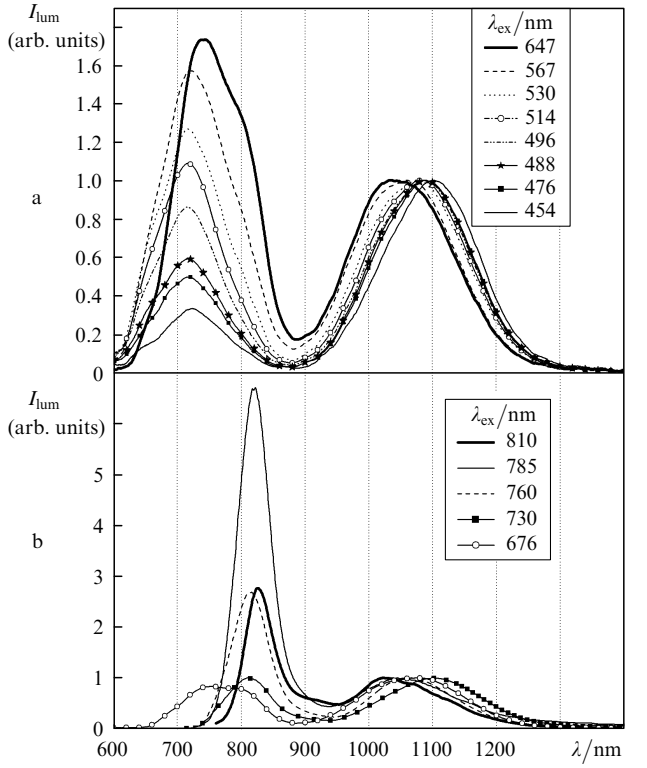

Figure 5. Effect of excitation wavelength on the red luminescence intensity for the bands at (a) 740 and (b) 810 nm. The spectra are normalised to the IR luminescence intensity.

In an earlier study [17], we determined the parameters of absorption and luminescence transitions and proposed a model involving three modifications (ABCs 1 – 3) of a bismuth centre in aluminosilicate glass. Consider the ratio of the number of photons absorbed and emitted by one modification to the total number of absorbed and emitted photons at a given wavelength:

$$\frac{N_{ABCi}}{N_{tot}} \sim \frac{M^{red}_{ABCi} + M^{IR}_{ABCi}}{M_{tot}}, \quad (1)$$

where N_{ABCi} is the number of absorbed photons; $i = 1, 2, 3$; $M^{red}_{ABCi} + M^{IR}_{ABCi}$ is the number of photons emitted in the red and IR luminescence bands for centre i; N_{tot} is the total number of absorbed photons; and M_{tot} is the total number of photons emitted in the fibre. Relation (1) is valid when nonlinear excited-state absorption and upconversion processes are left out of account [21, 22]. In view of this, our analysis relies on the luminescence spectra measured at low excitation powers, 10 – 15 mW.

The number of photons (M') emitted in a spectral range dv is related to the luminescence intensity $I_{lum}(v)$ by [23]

$$I_{lum}(v)dv = M'hvdv.$$

In the wavelength range dv, the luminescence intensity $I_{lum}(\lambda)$ was measured in units of power. Therefore,

$$I_{lum}(\lambda)d\lambda = \frac{I_{lum}(\lambda)}{v^2}\,dv = I_{lum}(v)dv.$$

The total number of photons emitted in the fibre is then

$$M_{tot} \sim \int \frac{I_{lum}(\lambda)}{v^3}\,dv.$$

The $I_{lum}(\lambda)/v^3$ spectra were fitted with six Gaussians (Γ_j), like in an earlier study [17]. According to the proposed model, each ABC has two radiative transitions, in the visible and IR spectral regions. Then, we have

$$M_{tot} \sim \int \frac{I_{lum}(\lambda)}{v^3}\,dv = \int \sum_{j=1}^{6} \Gamma_j dv$$

$$= \sum_{j=1}^{6} M_j = \sum_{i=1}^{3} \left(M^{red}_{ABCi} + M^{IR}_{ABCi}\right).$$

The parameters of the components were determined with an accuracy of 1 % – 3 %, which corresponded to an accuracy in our luminescence measurements in the order of 1 % – 5 % (depending on the spectral range).

The total number of absorbed photons, N_{tot}, is proportional to the absorption coefficient, α_{tot}, so the absorption spectra, $\alpha_{tot}(v)$, were fitted with nine Gaussians, Γ_k, because each ABC has three absorption transitions in the visible and IR spectral regions. Therefore,

$$N_{tot} \sim \alpha_{tot}(v) \sim \sum_{k=1}^{9} \Gamma_k(v) \sim \sum_{k=1}^{9} N_k \sim \sum_{i=1}^{3} N_{ABCi}.$$

Figure 6 shows the number of emitted photons as a function of excitation wavelength for the six Gaussian bands used to fit all the luminescence spectra. Comparison of the dependences obtained allows more accurate identification of the transitions of a given ABC. For example, the radiative transitions at 685 and 1148 nm are similar in the effect of excitation wavelength on the spectral dependence of the number of emitted photons; similar behaviour is exhibited by the sum spectrum of the absorption transitions at 460, 695 and 1010 nm. This leads us to assign this set of optical transitions to the same centre, ABC2. Analogous correlations can be made for ABC1 and ABC3.

In this way, we obtained the excitation spectra of the luminescence bands in terms of emitted photons, which are

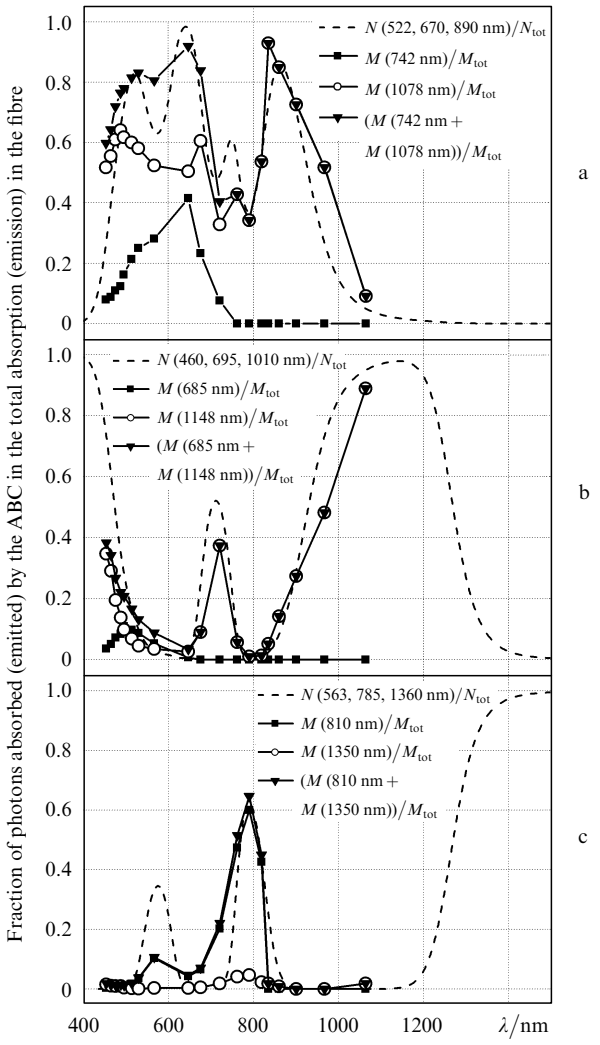

Figure 6. Ratio of the number of photons (N_{ABCi}) absorbed and emitted ($M^{red}_{ABCi} + M^{IR}_{ABCi}$) by (a) ABC1, (b) ABC2 and (c) ABC3 to the total number of photons absorbed (N_{tot}) and emitted (M_{tot}) in the fibre as a function of excitation wavelength. The numbers in brackets specify the spectral position of the absorption or emission band.

proportional to the normalised absorption spectra for each ABC. The results were used to identify the set of absorption and luminescence transitions of each ABC and to refine the energy level diagrams proposed earlier for the three ABCs [17]. According to the present data, the 522-nm transition (S_3) corresponds to radiative transitions of ABC1, and the 460-nm transition (S_3), to radiative transitions of ABC2. The data obtained made it possible to more accurately fit the absorption spectra with Gaussians and to refine the spectral positions of the S_1 and S_2 levels of ABC1 and ABC2. The Gaussian components in the absorption spectra of each centre are similar in temperature variation, as before; namely, the intensities of the absorption bands of ABC1 decrease with increasing temperature, whereas those of ABC2 increase.

The similar variations of the number of emitted photons with excitation wavelength for the transitions at 742 and 1078 nm suggest that these transitions belong to ABC1 (Fig. 6). Similarly, the 685-nm transition corresponds to the 1148-nm radiative transition of ABC2.

Excitation of bismuth-doped aluminosilicate fibres at 1350 nm has recently been shown to produce a luminescence

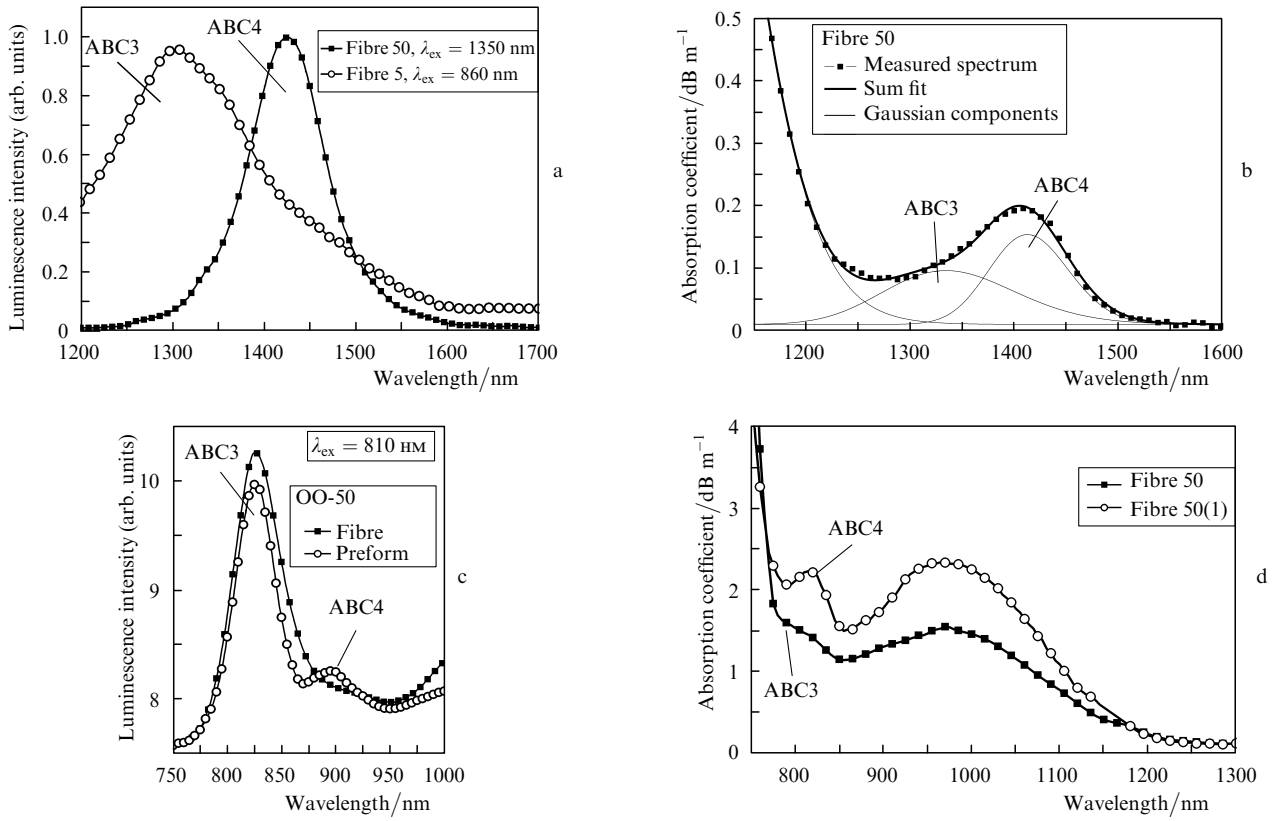

Figure 7. Luminescence spectra of fibres 5 [24] and 50 in the ranges (a) 1200 – 1700 and (c) 750 – 1000 nm. (b) Absorption band at 1400 nm in the loss spectrum of fibre 50 and a fit to the data with Gaussians. (d) Optical loss spectra of the single-mode fibres 50 and 50(1), drawn out from the same preform at different temperatures.

band centred at 1430 nm [2]. This band differs from the corresponding band of ABC3 (Fig. 7a). The broad absorption band (1400 nm) responsible for the 1430-nm luminescence considerably overlaps with the absorption peak of OH groups (1390 nm), which impedes its identification. In view of this, to determine the exact shape of the bismuth band, the absorption spectrum of fibre U16, free of bismuth and similar in parameters to the bismuth-doped fibre, was subtracted from the absorption spectrum of the latter. The difference spectrum was fitted with the smallest number of Gaussians needed to reach fit accuracy comparable to the measurement accuracy (Fig. 7b). As seen, the broad absorption band around 1400 nm is composed of two components located at 1335 and 1413 nm. The former corresponds to the 1350-nm luminescence band (ABC3), and the latter, corresponding to the 1430-nm luminescence band, seems to be due to an additional centre, ABC4.

As mentioned above, at excitation wavelengths in the range 730 – 810 nm the luminescence spectrum of sample OO-50 shows a band centred at 900 nm. This band is well seen in the spectrum of the preform and can be revealed in the spectrum of the fibre by decomposition into components (Fig. 7c)

Note that the spectral position of the bands of the ABCs is essentially independent of the fibre fabrication method, process parameters and fibre composition. The only exception is the 800-nm absorption band, whose position varies from sample to sample in the range 780 – 830 nm. For example, the spectra of the single-mode fibres 50 and 50(1), drawn out from the same preform at different temperatures (Fig. 7d), differ in the shape of this band. This indicates that the absorption band at $\sim$ 800 nm is composed of several components. Accordingly, its shape depends on the intensity of its components at $\sim$ 780 and 825 nm. These components in the absorption spectra of ABC3 and ABC4 correspond to the luminescence bands at 810 and 900 nm.

Thus, given that the absorption and luminescence bands of ABC1 – ABC3 were determined from the excitation spectra (Fig. 8), it is reasonable to assume that the luminescence bands at 900 and 1430 nm and the corresponding absorption bands at 825 and 1413 nm are due to ABC4. However, any absorption band that would correspond to the transition to the upper excited state and be an analogue of transitions of ABC1 – ABC3 has not yet been detected.

The data obtained can be used to construct four energy level diagrams, identical in structure and differing only in position and width (Fig. 8). Given that these diagrams are identical in energy level structure and similar in transition energies, we assume that they represent four modifications of a bismuth centre. One possible basic model of a bismuth centre is a BiO_4 tetrahedron whose molecular energy level diagram results from the intermixing of the Bi s-, p- and d-states with the s- and p-states of the oxygen ligands and is in qualitative agreement with experimental data [13]. The position of the molecular levels in this model depends significantly on the symmetry of the crystal (electric) field around the BiO_4 tetrahedron. The fact that all the absorption and luminescence bands can be divided into four distinct groups suggests that the ABCs in the aluminosilicate glass network have four types of environments.

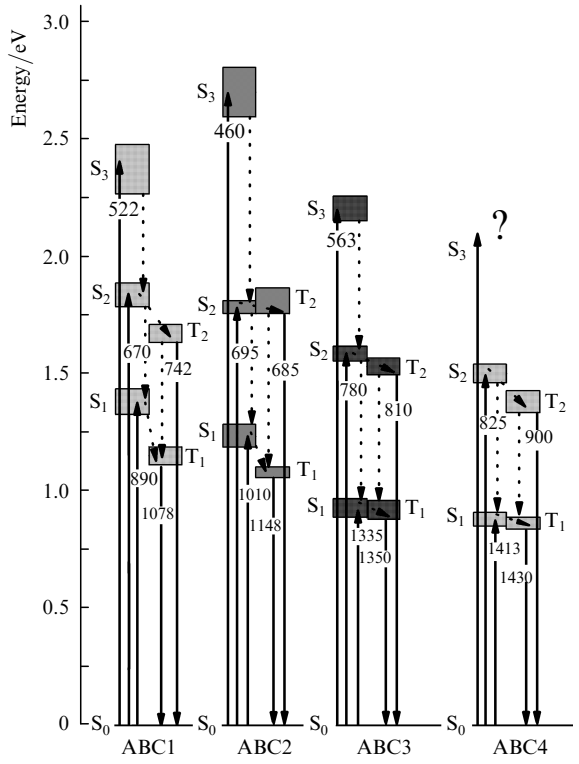

Figure 8. Energy level diagram of ABC1 – ABC4 in aluminosilicate glass. The height of the rectangles represents the width of the absorption and luminescence bands, the solid lines represent absorption and emission transitions, the dotted lines represent nonradiative transitions, and the numbers specify the wavelengths of the transitions in nanometres.

The intensity, shape and spectral position of the absorption and luminescence bands of the centres in aluminosilicate glass fibres depend on the aluminium concentration in their silicate core. In particular, with increasing aluminium concentration the absorption and luminescence bands shift to shorter wavelengths, which points to an increase in the strength of the IR transitions of ABC1 relative to ABC2 (Fig. 9). At low aluminium concentrations, the latter is located in an $AlO_{4/2}$ tetrahedral complex, predominantly in fourfold coordination. Increasing the aluminium concentration in the silicate glass favours the formation of $AlO_{6/2}$ octahedral structures, with the aluminium in sixfold coordination [25]. The increase in ABC1 concentration with aluminium content may be interpreted as evidence that the environment of this centre includes six-coordinate aluminium ions as second neighbours of the bismuth atom. The spectroscopic properties of ABC2 are in turn determined by the effect of the four-coordinate aluminium present in the $AlO_{4/2}$ tetrahedral complex.

Bismuth-doped germanosilicate fibres [15] and glass [26] have absorption and luminescence bands similar to those of ABC3 and ABC4 in aluminosilicate glass, in particular, a broad luminescence band in the range 1250 – 1600 nm, centred at 1425 – 1435 nm, with an excited-state lifetime of 310 – 360 μs. It is therefore reasonable to assume that the optical properties of ABC3 and ABC4 are unrelated to aluminium and are determined by the network of the silica glass, made up of rings of silicon-oxygen tetrahedra differing in the number of Si – O – Si linkages (from 2 to 11). Silica glass is known to consist mainly of medium rings (five to seven units), with low percentages of small (three- and four-membered) and large (eight- to ten-membered) rings [27]. It seems therefore likely that the bismuth-oxygen tetrahedra are incorporated predominantly into five- to seven-membered rings. The formation and spectroscopic properties of ABC3 and ABC4 may be governed by the effect of the less abundant small rings because these most severely distort the symmetry of neighbouring bismuth-containing medium rings [28]. The symmetry of the environment is known to have a strong effect on the luminescent properties of bismuth [29]. For example, when the structure of Y_2O_3 rings surrounding bismuth changes from symmetrical (S_6) to asymmetric (C_2), the blue-green luminescence band of Bi^{3+} shifts by $\sim$ 100 nm [30].

Two types of bismuth centres in fibre core glass were also identified by Truong et al. [19]. One of them is thermally

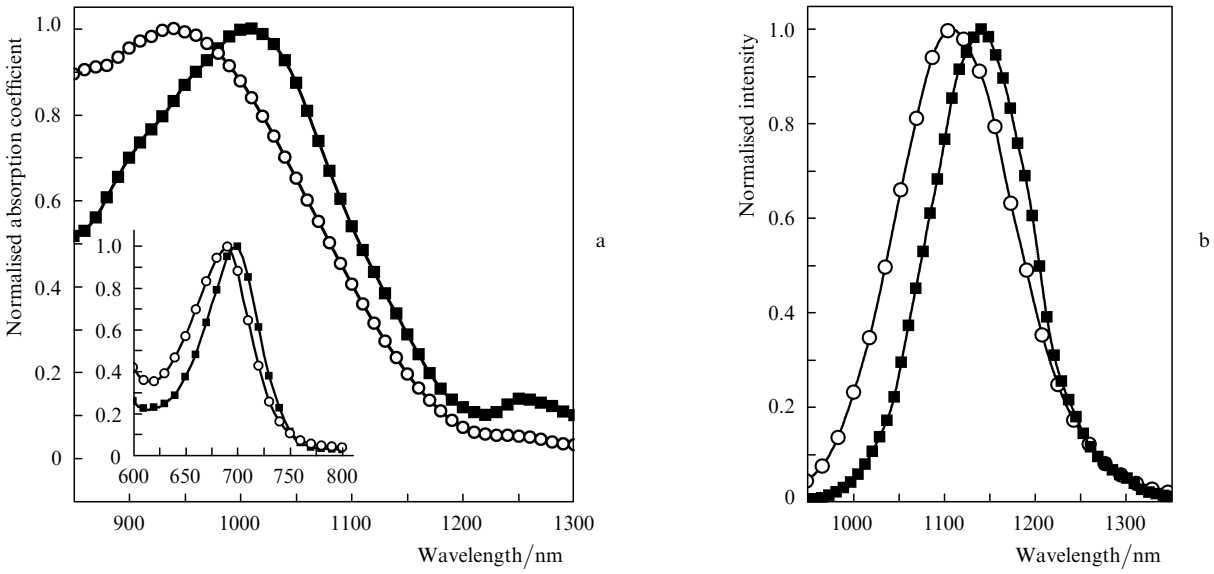

Figure 9. Effect of alumina concentration on the spectral position and shape of the (a) absorption and (b) luminescence bands of bismuth centres in aluminosilicate glass: 1.8 mol % (■) and 7 mol % (○) alumina; excitation wavelength, 1064 nm.

unstable and may be related directly to the silica host. High-temperature processing suppresses its luminescence around 1300 nm. The other, with a luminescence band near 1150 nm, is stable, and its stabilisation is due to the effect of aluminium.

All the above indicates that the nearest neighbour environment of a bismuth atom in the aluminosilicate glass network may include several structural units, which are responsible for the rather complex, but decodable, spectroscopic behaviour of the bismuth centres. Further work is however needed to accurately determine the structure of the ABC and assess the effect of the nearest neighbour environment on its properties.

4. Conclusions

The luminescence spectra of bismuth-doped aluminosilicate glass fibres were measured at various excitation powers and wavelengths. The saturation intensities of the luminescence bands at 742 and 1078 nm were determined to be ~ 70 and 3 kW cm^{-2}, respectively. The shape and spectral position of the luminescence bands were shown to depend on excitation power and wavelength, which indicates that both the red and IR luminescence bands are composed of several components. We identified a new luminescence band, centred at 900 nm, and a strong band at 810 nm under excitation in the range 730 – 810 nm.

Excitation spectra were obtained for each component of the luminescence spectrum. From comparison of the excitation and absorption spectra, we identified four types of active bismuth centres and sets of three absorption and two luminescence transitions of each centre. A diagram of energy levels and transitions is deduced for the four active bismuth centres.

The four types of centres are identical in energy level structure and similar in quantitative parameters of optical transitions, which leads us to view them as modifications of a single bismuth centre in aluminosilicate glass. The distinctions between the centres are related to the effect of different environments in the glass network. The optical properties of two centres are governed by the effect of aluminium ions in different coordinations, and those of the other two centres seem to be determined by the structure of the silica glass network, made up of rings of silicon-oxygen tetrahedra differing in the number of linkages.

Acknowledgements. We are grateful to A.A. Umnikov (Institute of Chemistry of High-Purity Substances, Russian Academy of Sciences) for fabricating the fibres and to S.V.Lavrishchev and L.D. Iskhakova (Fiber Optics Research Center) for determining the chemical composition of the samples. This work was supported in part by the Russian Foundation for Basic Research (Grant Nos 07-02-13598 and 08-02-12153).

References

1. Dianov E.M., Dvoyrin V.V., Mashinsky V.M., et al. *Kvantovaya Elektron.*, **35**, 1083 (2005) [*Quantum Electron.*, **35**, 1083 (2005)].
2. Dvoyrin V.V., Mashinsky V.M., Medvedkov O.I., et al. *Kvantovaya Elektron.*, **39**, 583 (2009) [*Quantum Electron.*, **39**, 583 (2009)].
3. Bufetov I.A., Dianov E.M. *Laser Phys. Lett.*, **6** (7), 487 (2009).
4. Dvoyrin V.V., Mashinsky V.M., Dianov E.M. *IEEE J. Quantum Electron.*, **44** (9), 834 (2008).
5. Zhou S., Feng G., et al. *J. Mater. Res.*, **22** (6), 1435 (2007).
6. Ren J., Yang L., Qiu J., Chen D., Jiang X., Zhu C. *Sol. State Commun.*, **141**, 559 (2007).
7. Ohkura T., Fujimoto Y., Nakatsuka M., Young-Seok S. *J. Am. Ceram. Soc.*, **90**, 3596 (2007).
8. Khonthon S. et al. *J. Ceram. Soc. Jpn.*, **115**, 259 (2007).
9. Sokolov V.O., Plotnichenko V.G., Koltashev V.V., Dianov E.M. *J. Phys. D: Appl. Phys.*, **42**, 095410 (2009).
10. Murata T., Mouri T. *J. Non-Cryst. Sol.,* **353**, 2403 (2007).
11. Peng M., Wu B., Da N., et al. *J. Non-Cryst. Sol.,* **354**, 1221 (2008).
12. Dvoyrin V.V., Mashinsky V.M., et al. in *Proc. 31st ECOC* (Glasgow, Scotland, 2005) Paper Th 3.3.5.
13. Kustov E.F., Bulatov L.I., et al. *Opt. Lett.*, **34** (10), 1549 (2009).
14. Ren J., Dong G., et al. *J. Phys. Chem. A*, **112** (14), 3066 (2008).
15. Qiu Y., Shen Y. *Opt. Mater.*, **31** (2), 223 (2008).
16. Fujimoto Y., Nakatsuka M. *Jpn. J. Appl. Phys.*, **40**, L279 (2001).
17. Bulatov L.I. et al. *Izv. Akad. Nauk, Ser. Fiz.*, **72** (12), 1754 (2008) [*Bull. Russ. Acad. Sci.; Phys.*, **72** (12), 1655 (2008)].
18. Razdobreev I., Bigot L., et al. *Appl. Phys. Lett.*, **90**, 031103 (2007).
19. Truong V.G., Bigot L., et al. *Appl. Phys. Lett.*, **92**, 041908 (2008).
20. Blasse G., Meijerink A., et al. *J. Phys. Chem. Sol.*, **55**, 171 (1994).
21. Kalita M.P., Yoo S., Sahu J. *Opt. Express*, **16** (25), 21032 (2008).
22. Bufetov I.A., Firstov S.V., Khopin V.F., Guryanov A.N., Dianov E.M., in *Proc. ECOC2008* (Brussels, Belgium, 2008) Paper Tu 3.B.4.
23. Levshin L.V., Saletskii A.M. *Lyuminestsentsiya i ee izmereniya* (Luminescence and Related Measurements) (Moscow: Mosk. Gos. Univ., 1989) p. 16.
24. Dvoyrin V.V., Mashinsky V.M., et al. *Opt. Lett.*, **31**, 2966 (2006).
25. Sen S., Stebbins J.F. *J. Non-Cryst. Sol.,* **188**, 54 (1995).
26. Neff M., Romano V., Luthy W. *Opt. Mater.*, **31** (2), 247 (2008).
27. Rino J.P., Ebbsjo I., et al. *Phys. Rev. B*, **47** (6), 3053 (1993).
28. Uchino T., Kitagawa Y., Yoko Y. *Phys. Rev. B*, **61** (1), 234 (2000).
29. Kustov E.F. et al. *J.Phys.B: At., Molec. Opt. Phys.*, **45**, 025402 (2010).
30. Van De Craats A.M., Blasse G. *Chem. Phys. Lett.*, **243**, 559 (1995).